Anomalous molecular orbital variation upon adsorption on a wide band gap insulator

ARTICLE *in* THE JOURNAL OF CHEMICAL PHYSICS · JUNE 2010

Impact Factor: 2.95 · DOI: 10.1063/1.3431755 · Source: PubMed

4 AUTHORS, INCLUDING:

Wei Chen
École Polytechnique Fédérale de Lausanne
32 PUBLICATIONS **262** CITATIONS
SEE PROFILE

Christoph Tegenkamp
Leibniz Universität Hannover
104 PUBLICATIONS **1,121** CITATIONS
SEE PROFILE

Herbert Pfnür
Leibniz Universität Hannover
214 PUBLICATIONS **4,331** CITATIONS
SEE PROFILE

Insight from First-Principles Calculations into the Interactions between Hydroxybenzoic Acids and Alkali Chloride Surfaces

Wei Chen,[†] Christoph Tegenkamp,[†] Herbert Pfnür,*[,†] and Thomas Bredow[‡]

Institut für Festkörperphysik, Leibniz Universität Hannover, 30167 Hannover, Germany, and Institut für Physikalische und Theoretische Chemie, Universität Bonn, 53115 Bonn, Germany

Received: September 28, 2009; Revised Manuscript Received: November 18, 2009

Tuning of effective band gaps at insulator surfaces by adsorbed molecules is of fundamental interest but also technologically relevant for contact charging induced by adsorbed molecules like hydroxybenzoic acids. Our studies by density functional theory of the adsorption of benzoic acid (BA), salicylic acid (SA), and para-salicylic acid (*p*-SA) on perfect KCl and NaCl(100) surfaces as well as on polar and nonpolar step edges reveal the importance of polar defects in this context. We also found that the van der Waals dispersion contributes to about half of the adsorption energy in most cases. Therefore, the van der Waals interaction must be explicitly taken into account even for the interaction between molecules and wide band gap insulator surfaces, respective of the adsorption on flat or stepped surfaces. On the other hand, the adsorption geometry is still determined by short-range forces, that is, by the weak chemical bonds and electrostatic interactions. These short-range interactions are mostly mediated by resonant coupling between HOMO-1 and HOMO-2 molecular states and the valence band of the solid, which results in very similar adsorption energies of these molecules on the KCl and NaCl surfaces. The interaction strength is significantly modified only at defects with large dipole moments (e.g., pairs of polar steps) resulting in split-off edge states below the valence band. Resonant coupling to these states leads to an almost rigid down-shift of all molecular orbitals that efficiently reduces the effective band gap at the surface. As a result, an effective band gap of 0.9 eV has been achieved on the polar KCl [011] stepped surface thanks to the relatively small HOMO−LUMO gap of SA.

Introduction

The understanding of the interactions between organic molecules and wide band gap insulators is of fundamental relevance both from a fundamental point of view and with respect to potential applications in various fields. For example, they serve as the building blocks for organic electronics and optoelectronic devices.[1−4] An even more intriguing example is the controlled contact charging of mineral salts induced by adsorption of submonolayers of small organic acid molecules like salicylic acid (SA).[8] This process, allowing the electrostatic separation of, for example, sodium chloride from potassium chloride on a large scale, turns out to be chemically highly selective. This means that chemcially very similar molecules like benzoic acid (BA) turn out to be much less efficient for electrostatic separation, whereas the change from ortho- to para-SA (*p*-SA) switches off the contact charging effect completely for this combination of salts.[6] This selectivity can only be understood by quantitative studies of the adsorption properties of these molecules.

It is obvious that efficient contact charging requires a (small) concentration of mobile charges but with relatively low mobility so that separation of charges is possible with sufficient probability. The latter property will most likely be fulfilled if charges are exchanged within the electronic states of submonolayers of organic molecules adsorbed on insulating surfaces in contact with each other. The first step, however, the generation of (potentially) mobile charges by thermal excitation, is more critical. It is obvious that there is no thermal excitation of electrons in wide band gap insulators. Only a proper alignment of the unoccupied molecular states during the adsorption of the molecules on the insulating surfaces with respect to the valence-band edges of the insulating material may effectively reduce the band gap at the interface.[6] Because this alignment depends both on intramolecular properties and on details of the adsorption, it provides a plausible reason for the different efficiencies of chemically similar molecules.[9] On the other hand, by exploiting the variability of organic molecules and their adsorption strength also on insulators, a new possibility for tailoring the effective band gap of the adsorbate system exists.[5−7]

This alignment of molecular orbitals is also susceptible to surface defects. Indeed, our previous studies indicate that, by adsorption of BA and its hydroxylated derivatives on perfect (100) surfaces of NaCl, the effective band gap of the adsorbate system is reduced to the energetic difference between the highest occupied molecular orbital (HOMO) and the lowest unoccupied molecular orbital (LUMO) of the adsorbed molecule, but this difference is around 5 eV.[5,7] This rules out the possibility that the contact charging effect will be effective on perfect NaCl and KCl surfaces and leads to the conclusion that surface defects must even play a major role in this process. Because the identification of various types of defects from experiment is extremely tedious, if not impossible, we started to carry out density functional first-principles calculations[7] on these surface with and without defects. As shown there, stronger bonds together with the appropriate alignment of electronic levels can indeed be mediated by surface defects, specifically those with polar character.[7]

* To whom correspondence should be addressed. E-mail: pfnuer@fkp.uni-hannover.de.
[†] Leibniz Universität Hannover.
[‡] Universität Bonn.

10.1021/jp909308k
Published on Web 12/08/2009

In order to get a quantitative description for weakly bound systems, the van der Waals (vdW) interaction should be included. Although standard density functional theory (DFT) is useful in predicting structures and electronic properties of systems characterized by strong chemical bonds, it has been well established that standard approximations, that is, local density approximation (LDA) and generalized gradient approximation (GGA), are local and semilocal in nature, and thus, they are incapable of capturing the long-range dispersion due to instantaneous polarizations in weakly bound systems.[10] Indeed, we have recently shown that the vdW interaction plays an important role for the binding of SA on NaCl(100).[11] Therefore, one should not neglect the long-range dispersion when treating the adsorption of conjugated organic molecule on an insulating surface, even in the case of large band gaps.

On the basis of the motivation given above, we present here a comprehensive study dedicated to the adsorption of BA and two hydroxybenzoic acids, namely, SA and *p*-SA on KCl surfaces with the long-range vdW interaction taken into account in DFT calculations. On the basis of the experience gathered by the investigation of adsorption of these molecules on the NaCl surfaces,[7] we concentrate here on a comparison of adsorption geometries and electronic structures on the ideal KCl(100) surface with that on a surface with [011]-oriented pairs of polar steps, which are taken as surface model systems. These results will be discussed in conjunction with the adsorption on the NaCl surface in order to obtain a detailed picture of the interactions between the hydroxybenzoic acids and alkali chloride surfaces but also to get general insights into the mechanism of an ubiquitous phenomenon like contact charging.

Computational Methods

To correct the band-gap underestimation issue within standard DFT approximations, we carried out the periodic DFT calculations by using the PW1PW hybrid exchange−correlation (XC) functional[12] with the linear combination of atomic orbitals (LCAO) code CRYSTAL06.[13] The mixing of 20% exact Hartree−Fock (HF) exchange with the Perdew−Wang 91 (PW91) generalized gradient approximation (GGA) exchange in the PW1PW hybrid functional shows significant improvement of the structural and electronic properties of NaCl and some oxides.[7,12] The multielectronic atomic wave function in CRYSTAL06 is constructed as a Slater determinant of Bloch functions which are linear combinations of Gaussian-type functions. In the present study, K and Cl are expanded by the 86-511G and 86-311G split-valence basis sets, respectively.[14] For various hydroxybenzoic acids, C, O, and H atoms are described with the Pople-type 6-31G(d) basis sets. The molecule-KCl(100) system is modeled with two-sided adsorption on a (3 × 3) supercell with a five-layer thick slab. The [011]-oriented step is constructed from a four-layer KCl(100) slab extended to a (7 × 4) supercell, the step edges of the first layer of which run along the $\langle 0\bar{1}1\rangle$ direction. Detailed PW1PW calculation parameters can be found in ref 7.

We applied two different approaches to account for the missing long-range dispersion force in the standard DFT calculations: the empirical DFT-D method and the ab initio vdW density functional (vdW-DF). The dispersion corrected DFT-D energy based on Grimme's implementation is the sum of the Kohn−Sham (KS) DFT energy and the empirical correction

$$E_{\mathrm{DFT-D}} = E_{\mathrm{KS-DFT}} + E_{\mathrm{disp}} \tag{1}$$

where the empirically corrected term E_{disp} is defined as:[15]

$$E_{\mathrm{disp}} = -s_6 \sum_{i=1}^{N-1} \sum_{j=i+1}^{N} \frac{C_6^{ij}}{R_6^{ij}} f_{\mathrm{damp}}(R_{ij}) \tag{2}$$

C_{ij} and R_{ij} are the dispersion coefficients and interatomic distances for atom pair *ij*, respectively. s_6 is a global scaling factor, which is empirically set to 0.75 for the Perdew−Burke−Ernzerhof (PBE) functional. The damping function f_{damp} given by

$$f_{\mathrm{damp}}(R_{ij}) = \frac{1}{1 + e^{-\alpha(R_{ij}/R_0 - 1)}} \tag{3}$$

serves to cut off the unreasonable behavior of the asymptotic vdW interaction for small R_{ij}. R_0 is the sum of modified atomic vdW radii, and α is a global parameter.

This DFT-D method has been recently implemented in the plane-wave VASP code.[16−18] Here, we use the PBE XC functional[19,20] (PBE-D) with the projector augmented wave (PAW) method within the frozen-core approximation to retain information about the core electrons.[21,22] For a straightforward impression of the effect of the vdW interaction, we have also conducted calculations with the standard PBE functional without dispersion. In DFT-D, full geometric optimization is achieved analytically through the evaluation of the first derivative of the empirical dispersion energy. As usual, we switched off the intrafragment dispersion correction and only applied the correction between the adsorbate and the surface because the chemical interaction dominates for the local bonding of both the organic molecule and alkali chloride surface. The plane-wave basis-set kinetic cutoff energy is 450 eV throughout the PBE and PBE-D calculations. In particular, the adsorption of various BAs on KCl(100) uses single-sided adsorption on a (4 × 4) surface supercell with a thickness of three atomic layers to minimize the intermolecular interaction. The periodically repeated images of the slab are separated by a sufficiently large vacuum region (≥18 Å). The Brillouin zone is sampled with a (2 × 2 × 1) Monkhorst-Pack (MP) *k*-point mesh. The bottom layers of both the (100) surface and the [011] stepped surface are held fixed during the geometric optimization, whereas the upper layers and adsorbate are allowed to relax until the atomic forces are less than 0.02 eV Å^{-1}.

As another approach to remedy the lack of vdW interaction in standard DFT approximations, the vdW-DF has been introduced into DFT by construction of a truly nonlocal correlation functional.[10,23] The vdW-DF XC energy is given as

$$E_{\mathrm{vdW-DF}} = E_{\mathrm{GGA,x}} + E_{\mathrm{LDA,c}} + E_{\mathrm{c}}^{\mathrm{nl}} \tag{4}$$

where the energy terms on the right-hand side represent the GGA exchange, LDA correlation, and nonlocal correlation energy, respectively. The dynamical long-range dispersion is therefore explicitly included as the non-nonlocal correlation effect. In the vdW-DF 04 version, the revPBE exchange is chosen as the GGA exchange because it is close to the HF exchange. Thus, it suffers least from the erroneous overbinding due to exchange alone compared to other exchange functionals.[10,23] The nonlocal correlation energy $E_{\mathrm{c}}^{\mathrm{nl}}$ can be calculated from

$$E_{\mathrm{c}}^{\mathrm{nl}} = \frac{1}{2} \int \int n(r)\, \phi(r, r')\, n(r')\, \mathrm{d}^3 r\, \mathrm{d}^3 r' \tag{5}$$

where the interaction kernel $\phi(r, r')$ depends on the density and its gradient. One can refer to ref 23 for the description of the kernel. Presently, we adopt the a posteriori energy-correction scheme within the vdW-DF by using the PBE-D optimized adsorption geometry as input. Although we have shown that self-consistent field vdW-DF can be applied on such systems

TABLE 1: Calculated Equilibrium Lattice Constant (a_0) and Band Gap (E_g) of KCl

parameters	PW1PW LCAO[a]	PBE PAW[b]	experiment
a_0 (Å)	6.48	6.39	6.20[c]
E_g (eV)	8.00	5.04	8.7[d]

[a] A (8 × 8 × 8) *k*-point mesh is used. [b] The cutoff energy is 750 eV. Force convergence criterium is 0.001 eV/Å. [c] Ref 26. [d] Ref 27.

with an efficient algorithm,[7,24] the computational cost is still much higher than that of the DFT-D method. For the vdW-DF calculations, we used the grid-based real space GPAW code with a grid spacing of 0.20 Å.[25] The Brillouin zone is accordingly sampled by a (2 × 2 × 1) *k*-point mesh.

To this end, the computation scheme used for this study involves several density functionals. The PW1PW hybrid functional is used to give a proper fundamental gap for the adsorbate system, whereas the PBE XC and revPBE exchange functional are coupled to two different implementations of vdW force in the DFT (i.e., PBE-D and vdW-DF), respectively. As we will show later, the PBE-D and vdW-DF yield similar binding strengths between the hydroxybenzoic acid and alkali halide surface, which implies that both methods are adequate for the evaluation of the long-range dispersion of such systems. The choice of slab thickness, size of unit cells, number of *k*-points, and so on has been optimized by test calculations in order to guarantee energetic convergence and negligible interactions between adsorbed molecules and slabs.

Results and Discussion

Bulk KCl Properties. We first checked the two basic parameters for the bulk KCl, that is, the equilibrium lattice constant (a_0) and the band gap (E_g), which are given in Table 1. It should be kept in mind that the experimental a_0 from ref 26 measured at room temperature includes zero-point phonon effects, which usually show an expansion of 1% compared to the 0 K value for the ionic solids.[28] Nevertheless, it is clear that both PW1PW hybrid functional and PBE GGA functional tend to overestimate the lattice constant of bulk KCl. In particular, the PBE functional outperforms the PW1PW with less overestimation (4.1%).

The band gap, on the other hand, can only be properly described by the PW1PW hybrid functional. The value yielded by the PBE is severely underestimated and is 42% smaller than the experimental gap. This is not astonishing because this is a systematic problem with standard DFT approximations inherited from self-interaction and derivative discontinuity of the XC potential. The addition of the nonlocal HF exchange to the GGA exchange manages to correct the band gap to some extent, leading to a much closer agreement with the experiment. The band structure predicted by PW1PW closely resembles that of bulk NaCl.[7] The valence band is mostly of Cl 3p character, and the lowest conduction band sees a mixture of the K 4s, and, more significantly, the Cl 4s states. The valence bandwidth is 0.94 eV, which is about 1 eV smaller than that of NaCl. Because the valence bandwidth is determined by second-neighbor p−p overlap, the smaller dispersion of the KCl valence band is a result of partial screening of the overlap, which stems from the higher degree of ionic bonding due to the higher electropositivity of K. This is also evidenced by the Mulliken population analysis that results in an absolute net atomic charge of KCl of 1.004 e for the ions, which is larger than that of bulk NaCl.

Hydroxybenzoic Acids on KCl(100). The adsorption study starts with the investigation of various hydroxybenzoic acids on the ideal KCl(100) surface as shown in Figure 1. The electronic structure of KCl(100) surface is, as expected, very close to that of the bulk without surface states. The calculated surface energy is 9.25 meV/Å with the PW1PW functional, which falls in line with other theoretical values and experiments.[29,30]

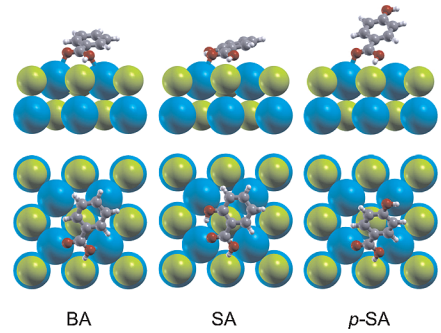

Figure 1. Side-view (top panel) and top-view (bottom) schematics of the adsorption of BA, SA, and *p*-SA on KCl(100) surface. Potassium atoms, blue; chlorine atoms, green; oxygen atoms, red; carbon atoms, gray; hydrogen atoms, white.

Two quantities, namely, adsorption energy (E_{ads}) and interaction energy (E_{int}), are introduced to measure the binding strength and the influence of long-range vdW contribution. They are defined as

$$E_{ads/int} = E_{system}^{relaxed} - E_{surface}^{relaxed/rigid} - E_{molecule}^{relaxed/rigid} \quad (6)$$

Here, $E^{relaxed}$ represents the energy of the corresponding fragment in its equilibrium geometry, whereas the coordinates are fixed at the values in the optimized surface−adsorbate system for E^{rigid}. Thus, E_{int} simply gives the impression of the interaction strength between the adsorbed molecule and the surface, whereas E_{ads} takes into account the energy required for the deformation of the molecule and surface from their isolated equilibrium configuration.

In Table 2, calculated adsorption and interaction energies are presented for the various adsorption systems on KCl(100), as well as on NaCl(100) for comparison. As seen there, the standard DFT methods employing the PW1PW hybrid functional and the PBE GGA functional yield quite similar E_{ads} because the two flavors of GGA, that is, the PW91 functional in PW1PW and PBE, are generally equivalent for many properties.[31−33] The adsorption energies on both surfaces are also very close, although on NaCl E_{ads} values are slightly larger.

The adsorption on KCl(100) follows the same configuration as that on NaCl(100) through the electrostatic interaction between the K−O and Cl−H bonds (see Table 3). The dominant chemical bonding occurs between the double-bonded carboxylic O and surface K atoms, with an average bond length of 2.8 and 2.7 Å by PW1PW and PBE, respectively. The partially covalent character of the K−O bond can be revealed by the charge density difference map (not shown) where the electrons are localized in the region between the two atoms joined by the bond. This is supported by the projected density of states (PDOS) in Figure 2 where the HOMO-1 and HOMO-2 of the adsorbate are smeared out as a result of the hybridizations between the $p_{x,y}$ (HOMO-2), p_z (HOMO-1) electrons of the molecule (see Figure 3), and the s band of surface K atoms. This can be qualitatively described within the Newns−Anderson model of adsorption in the weak chemisorption limit; that is, a single valence level of the molecule is broadened into a resonance with a finite lifetime.[34−36] Consequently, the carboxylic group is slightly rotated along the C=C bond with

TABLE 2: Adsorption Energies and Interaction Energies (in Parentheses) of BA, SA, and *p*-SA on KCl and NaCl(100) Surfaces[a]

			PBE-D			vdW-DF		
adsorbate	PW1PW[b]	PBE	total	PBE	vdW[c]	total	revPBE	XC diff.[d]
				On KCl(100)				
BA	−0.40	−0.44	−0.72 (−0.84)	−0.41 (−0.53)	−0.31	(−0.77)	(−0.27)	(−0.50)
SA	−0.43	−0.43	−0.84 (−1.04)	−0.43 (−0.63)	−0.41	(−0.99)	(−0.31)	(−0.68)
p-SA	−0.44	−0.44	−0.62 (−0.71)	−0.44 (−0.53)	−0.18	(−0.67)	(−0.36)	(−0.31)
				On NaCl(100)				
BA	−0.43	−0.44	−0.82 (−0.96)	−0.41 (−0.56)	−0.40	(−0.77)	(−0.25)	(−0.52)
SA	−0.48	−0.45	−0.98 (−1.19)	−0.45 (−0.66)	−0.53	(−0.94)	(−0.25)	(−0.69)
p-SA	−0.45	−0.45	−0.81 (−0.93)	−0.45 (−0.56)	−0.37	(−0.78)	(−0.27)	(−0.51)

[a] All energies are given in electron Volts (eV). [b] The reported energies have been corrected for the basis set superposition error (BSSE). [c] The vdW contributions to the adsorption energy and interaction energy are the same. [d] $\Delta E_{xc} = E_{LDA,c} + E_c^{nl} - E_{revPBE,x}$.

TABLE 3: Relaxed Geometric Parameters of BA, SA, and *p*-SA on KCl and NaCl(100)[a]

PW1PW				PBE				PBE-D			
R	ϕ_{tilt}	$d_{K(Na)-O}$	d_{Cl-H}	R	ϕ_{tilt}	$d_{K(Na)-O}$	d_{Cl-H}	R	ϕ_{tilt}	$d_{K(Na)-O}$	d_{Cl-H}
					On KCl(100)						
					Adsorbate: BA						
3.53	21.5	2.81	2.26	3.89	30.2	2.67	2.10	3.81	29.7	2.67	2.09
		2.88				3.12				3.06	
					Adsorbate : SA						
3.15	14.4	2.79	2.30	3.46	23.2	2.76	2.23	3.44	23.2	2.75	2.21
		2.99				3.28				3.20	
		(3.06)				(2.98)				(2.94)	
					Adsorbate: *p*-SA						
4.55	42.6	2.76	2.17	5.08	46.4	2.73	2.17	5.08	46.4	2.73	2.17
		2.99				3.85				3.85	
					On NaCl(100)						
					Adsorbate: BA						
3.82	30.5	2.37	2.18	3.86	29.9	2.32	2.10	3.80	30.9	2.36	2.03
		2.74				2.97				2.66	
					Adsorbate: SA						
3.49	31.3	2.37	2.31	3.45	29.2	2.38	2.16	3.41	28.6	2.38	2.12
		3.25				3.22				3.01	
		(2.50)				(2.57)				(2.54)	
					Adsorbate: *p*-SA						
3.89	29.1	2.37	2.19	4.01	29.9	2.31	2.10	4.00	30.2	2.32	2.08
		2.70				3.00				2.86	

[a] The separation R (in angstroms) is the distance between the geometric center of the molecule and the averaged position of the (100) surface. The tilt angle ϕ_{tilt} (in degres) is defined as the dihedral angle between the benzene ring and the (100) plane. $d_{K(Na)-O}$ (in angstroms) represents the distance from the carboxylic O to the nearest K (Na) atom. The interatomic distance between carboxylic H and Cl atoms is denoted by (d_{Cl-H}). The additional bond distance between phenolic O and surface K is shown in parentheses for the SA-adsorbate system.

respect to the benzene ring. Moreover, the hybridization between the in-plane $p_{x,y}$ orbital of the carboxylic group and K s valence states gives rise to a tilted molecular adsorption configuration.

Interestingly, it is clearly seen in Figure 1 and Table 3 that, on KCl(100), the adsorbed *p*-SA is significantly more rotated out of the surface plane as compared to both BA and SA. When inspecting the PDOS (not shown), one sees a rather pronounced broadening of both the HOMO-2 and HOMO-1 of *p*-SA. This strong HOMO-2 resonance in *p*-SA, which gives rise to a more upright adsorption configuration on KCl(100), is essentially caused by the small separation between the HOMO-1 and HOMO-2 (0.16 eV) as shown in Figure 3. Indeed, we find that the tilt angle for adsorption on KCl(100) is directly related to the energetic difference between the HOMO-1 and HOMO-2 of the adsorbate molecule: the smaller the separation between the HOMO-1 and HOMO-2 is, the more the molecule is tilted out of the surface plane. On the NaCl(100) surface, because of the broader Na 3s valence band and a more equal distribution of resonance states for all three molecules, the tilt-angle dependence is thus absent.

In the next step, geometric optimizations are performed within the dispersion-corrected PBE-D calculations to account for the missing vdW contribution in standard DFT approximations. Nevertheless, the final adsorption configurations for all molecules are very close to those obtained without dispersion corrections (see Table 3). This is in accordance with our previous self-consistent vdW-DF study on the SA−NaCl(100) system, which shows that the local chemical interaction turns out to be decisive for the optimal bonding geometry.[11] A close inspection shows a systematic decrease of the distance between the singly bound carboxylic O and surface K atoms after the dispersion is included, whereas the bond length between the doubly bound carboxylic O and K atoms is unaltered (see the first row of d_{K-O} in Table 3). One can also see that the PBE parts of the adsorption energy in PBE-D calculations are equivalent to the descriptions without dispersion. Specifically, a very small decrease (0.03 eV)

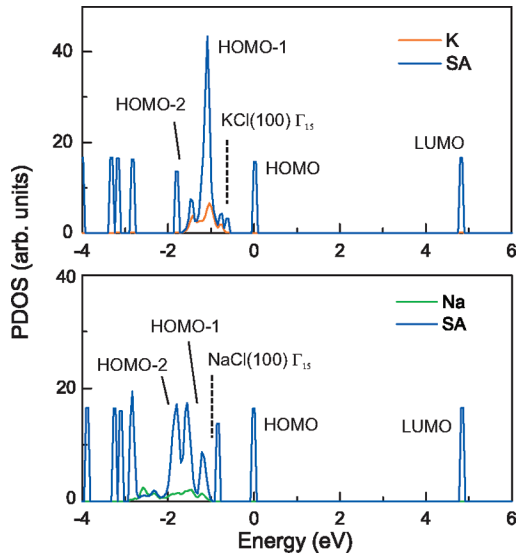

Figure 2. Comparison of the calculated density of states projected onto the SA molecule and onto the cations for adsorption on KCl (top) and NaCl(100) (bottom) surfaces with the PW1PW functional. The energy zero is shifted to the HOMO of SA.

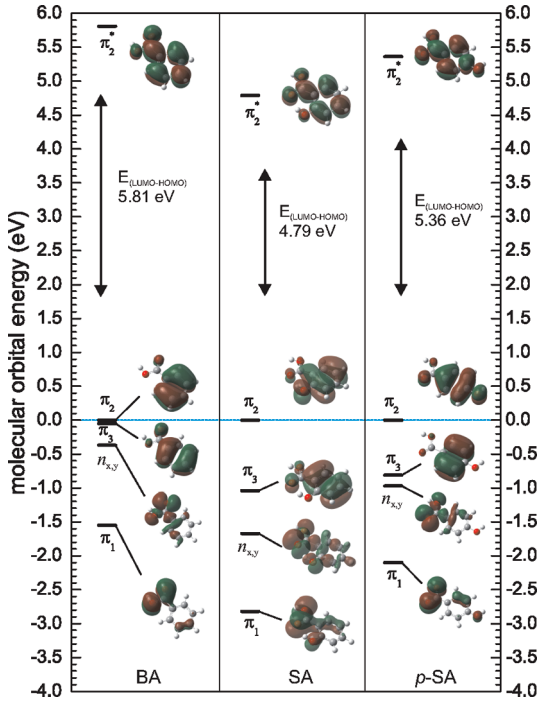

Figure 3. Diagrams of highest occupied and lowest unoccupied molecular orbital energy levels for BA, SA, and *p*-SA molecules calculated by PW1PW.

of the PBE E_{ads} for the BA-adsorbate system is found after the vdW interaction is taken into account. This suggests that the final optimal geometry is stabilized by the interplay of the local chemical interaction and long-range dispersion. In general, the whole molecule is closer to the surface as a result of the attractive vdW forces, but the change is rather subtle.

Although the effect on the adsorption geometry of the vdW interaction is small, it greatly enhances the binding to the surface. As seen from Table 2, the total E_{ads} increases by −0.2 to −0.5 eV because of the vdW contribution. Thus, the strength of the vdW interaction is comparable to the chemical interaction. Only for the *p*-SA−KCl(100) system, the magnitude of the vdW contribution is much smaller because the aromatic ring is further

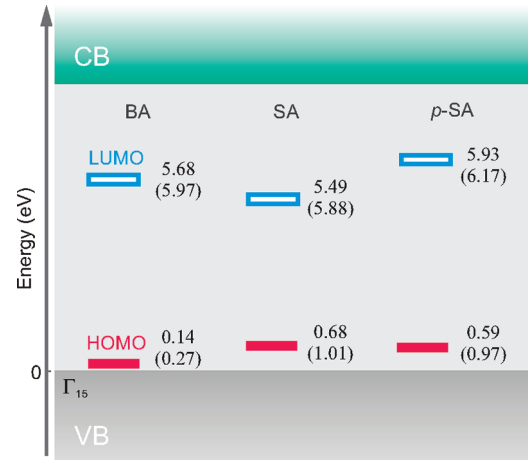

Figure 4. Band diagram of BA, SA, and *p*-SA adsorbed on the perfect KCl(100) surface, calculated with the PW1PW functional. The VBM of the surface defines energy zero. Values of adsorbate systems on NaCl(100) are also reported in parentheses.

away from the surface. When the vdW-DF is applied to the PBE-D optimized structure, it yields E_{int} values close to the PBE-D values. This should not be considered as a coincidence, because the PBE-D and vdW-DF are constructed from qualitatively different approaches. The well-known trend that revPBE systematically yields smaller binding energies than PBE and PW91,[31,37] is also found here (see Table 2). It should be pointed out that, although the choice of the revPBE exchange in the vdW-DF is generally appropriate, in some cases such as for the hydrogen-bonded complexes, it may underestimate the binding. Nevertheless, we show that the overall interaction energies agree well with the PBE-D method when the revPBE exchange is combined with the nonlocal correlation energy. It is thus reasonable to expect that both PBE-D and vdW-DF are capable of describing the long-range dispersion between the conjugated molecules and ionic insulators. In addition, we find that the SA-adsorbate systems yield the largest dispersion. Because the π electrons are delocalized over the whole molecule from the aromatic ring to the carboxylic and phenolic group, the enhanced vdW interaction can be explained by the contribution from the additional phenolic group in SA. The phenolic group in the *p*-SA-adsorbate system, on the other hand, is positioned quite far away from the surface, thus imposing a smaller effect on the interaction energy.

To address the effect of various hydroxybenzoic acids on the electronic structure of the adsorbate systems, the Kohn−Sham energy levels for adsorptions on KCl and NaCl(100) are compiled and presented in Figure 4. One should note that, although the PW1PW functional is used here for the prediction of the electronic structure, the overall picture is still valid, because we have shown that the inclusion of long-range dispersion has a limited effect on the band alignment between the adsorbate MOs and surface electronic states.[11] We see a systematic trend that the HOMO and LUMO of the adsorbate on KCl(100) surface is 0.2−0.4 eV closer to the valence-band maximum (VBM, Γ_{15} point) of the surface as compared to the adsorption on NaCl(100). Such a difference can be rationalized by the PDOS of the different surfaces given in Figure 2. We use the SA adsorbed system as an example, but an analogous discussion can be applied to the other systems. First, we see that the valence band of Na for the (100) surface is broader than that of K, which is consistent with the bulk. For adsorption on NaCl(100), the HOMO-2 couples more strongly to the surface Na valence band than the HOMO-1, whereas on

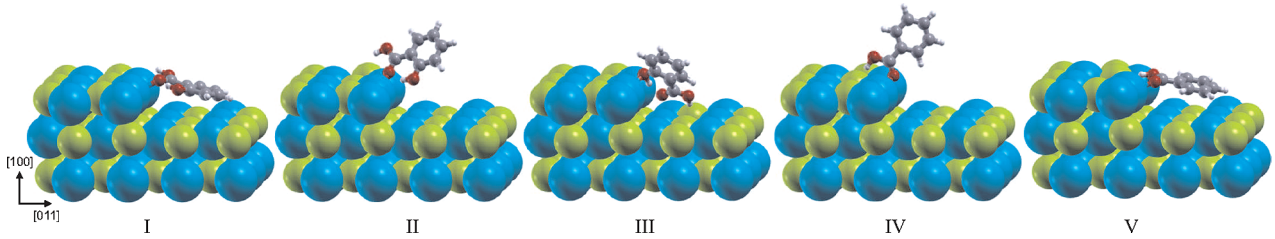

Figure 5. Adsorption sites of SA (I−III) and BA (IV, V) at the KCl [011] step with different configurations optimized by PBE-D.

KCl(100), the broadening of the HOMO-1 is more pronounced. Thus, the resonance between HOMO-1 and K valence band shifts the whole MOs of the molecule with respect to the surface, and it gives rise to a closer alignment between HOMO and Γ_{15} on KCl(100). Nevertheless, it is clear from the diagram that the effective band gaps for all systems are determined by the HOMO−LUMO separation. The HOMO−LUMO gaps stay almost identical after adsorption on KCl and NaCl; that is, they do not deviate significantly from the isolated state as a result of weak interactions.[7] As a general rule, we show that the electronic levels induced by the adsorption of various hydroxybenzoic acid on halide chloride (100) surface can reduce the effective surface band gap to the HOMO−LUMO separation of the adsorbate; albeit it is still too large for effective excitation by thermal energy.

Hydroxybenzoic Acids at the KCl [011] Step. So far, we have discussed the adsorption of various hydroxybenzoic acids on flat (100) surface of KCl and NaCl. In this section, we extend the study to the stoichiometric [011]-oriented step, which is one specific example of surface polar defects that could induce a substantial change in the electronic structure of the ionic solids. It generally cannot be achieved by other nonpolar defects, such as the [001] step.[7] Inspired by this unique effect, we adopt the monatomic [011] step model proposed in ref 7 and apply it to the KCl surface. The step edge of the [011] step is either terminated with Cl or K atoms. The alternating Cl−K−Cl− atomic rows give rise to a nonzero dipole moment along [01$\bar{1}$] because of the electrical field between the two neighboring atomic rows.[38−41] As a direct consequence, the total dipole moment is proportional to the number of the atomic rows along the step direction. Because the polarization of the stepped surface is closely related to its electronic structure, a small number of atomic rows will be too artificial wheares a large step width (or steps with kinks) are hard to treat because a much larger unit cell has to be used in order to minimize the electrostatic interaction between the step edges in neighboring cells. In the present calculations, we use a stepped surface with [011]-oriented steps and a step width of six atomic rows, the electronic structure of which has been demonstrated to be comparable to the models with larger step width. Its ledge energy, according to the definition in ref 7, is 199 meV/Å calculated by PW1PW, similar to the value of the NaCl [011] step (209 meV/Å). As a consequence of the reduced Madelung potential at the step edge and of atomic relaxations at the steps, edge states appear in the bulk band gap, which reduce the effective band gap by 3.7 eV compared to the bulk value. This reduction is accompanied by the upshift of the 3p band from the step-edge Cl atoms with respect to the Γ_{15} point. As a result, the top of the valence band is now mainly comprised of the 3p electrons localized at the step-edge Cl atoms.

We now place molecules at the K-terminated step edge, which is expected to be energetically more favorable than at the Cl-terminated side.[7] Compared to the ideal (100) surface, the surface with monatomic [011] steps apparently leads to a larger number of possible adsorption geometries for the hydroxybenzoic acids. We have tested several adsorption configurations by placing the molecule on the step edge and on the lower terrace with different orientations. In Figure 5, three representative adsorption configurations for the SA-adsorbate system are illustrated.

TABLE 4: Molecular E_{ads} (in Electronvolts) for Various Adsorption Configurations at the KCl [011] Step Edge Calculated by PBE-D[a]

configuration	total[b]	PBE	vdW
	SA		
I	−0.68	−0.23	−0.45
II	−0.38	−0.15	−0.23
III	−1.10	−0.67	−0.43
	BA		
IV	−0.99	−0.76	−0.23
V	−0.98	−0.47	−0.51

[a] The configurations refer to Figure 5. [b] The *k*-points are sampled with a (2 × 2 × 1) MP mesh.

The corresponding adsorption energies calculated with the PBE-D method are given in Table 4, including the contributions from the PBE functional and the vdW interaction. One can clearly see that the structure III in Figure 5 is the preferred adsorption configuration where the carboxylic group points toward the lower terrace of the (100) surface and the phenolic O is in close proximity to the undercoordinated K atom at the step edge. This is also the optimal adsorption geometry predicted by the PW1PW functional. Although this configuration has the largest energy gain already from the GGA part, we show in Table 4 that the long-range vdW interaction is again rather large and comparable to structure I, where the molecule lies closer to the low-lying (100) terrace. It is obvious that the long-range dispersion further stabilizes the adsorption of SA at the step edge for structure III, making it the preferred adsorption configuration overall. Thus, the inclusion of vdW forces does not change the trends set by the chemical interactions. It should be noted that in structures I and II, the vdW interaction is predominant for the molecular adsorption, whereas in structure III, we find a larger local electrostatic contribution to the adsorption energy. When turning to the adsorption of BA molecule, one can see that the GGA functional yields the structure IV in Figure 5 in which the adsorbate binds to the step edge site in an upright configuration. The inclusion of dispersion, however, gives rise to another flat configuration on (100) terrace with almost the same adsorption energy as that of the standing-up configuration (see Table 4). Obviously, different from structure IV, the vdW interaction is now predominant because of the close proximity between the molecular plane and the low-lying surface, which compensates for the smaller electrostatic interactions in the flat configuration. This indicates that at low coverage, both configurations IV and V are energetically equivalent for the adsorption of BA at the [011]-stepped surface despite of their different bonding mechanisms.

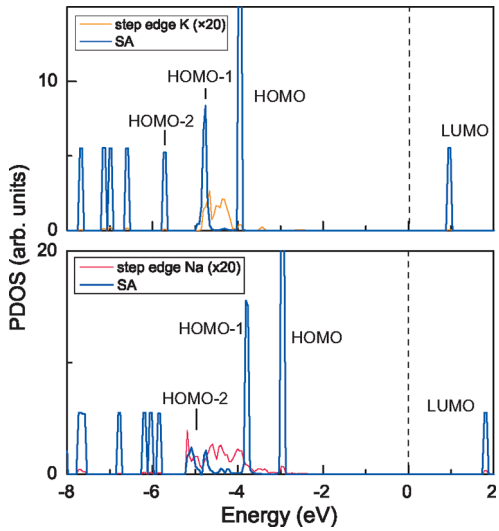

Figure 6. PDOS calculated with the PW1PW functional, projected onto SA and step-edge cation states for adsorption of SA at KCl and NaCl [011] steps. The top of the stepped surface valence band is shifted to energy zero.

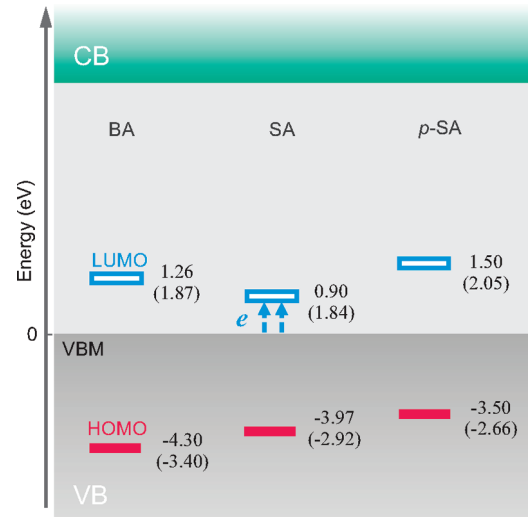

Figure 7. Band diagram of BA, SA, and *p*-SA adsorbed at the KCl [011] step edge calculated with the PW1PW functional. The KS eigenstates of the adsorbates are shifted with respect to the VBM of the stepped surface. The energy levels on the corresponding NaCl surface are presented in parentheses.

Nevertheless, in general, the adsorption geometry is still largely governed by the local bonding environment. By using the PW1PW1 hybrid functional, we find E_{ads} of −0.89, −0.97, and −0.94 eV for the BA, SA, and *p*-SA-adsorbate systems at the KCl [011] step edge including BSSE correction, respectively. In accord with the results at the NaCl [011] stepped surface, these larger E_{ads} with respect to the adsorption on flat (100) surface generally stem from the stronger binding between the O atom and the undercoordinated cation at the step edge.

We now move to the electronic structure of the adsorption on KCl [011] stepped surface. At first glance, when looking at the PDOS shown in Figure 6, the separation between the top of the valence band and the LUMO of the adsorbate is about 1 eV closer than that on the NaCl counterpart. The origin of the discrepancy is clearly revealed in the PDOS by the different resonance states between the adsorbate MO and the surface valence band from the step edge cations. Although the HOMO-2 and, to some extent, HOMO-1 are broadened by the adsorption on NaCl, it is apparent that on KCl, the HOMO-2 remains as sharp as in the isolated molecule, leaving only the HOMO-1 in resonance with the valence states from the step-edge cations, which subsequently shifts the whole MOs and aligns the LUMO closer to the top of the valence band. This is in agreement with what has been found on flat (100) surface where the HOMO-1 broadens more evidently than the HOMO-2 for KCl surface. It should be noted that compared to the adsorption on (100) surface, the MOs of the adsorbate experience a much larger shift from their original position than in the free molecule because of the polarity of the step. As expected, the effective band gaps for BA and *p*-SA adsorbed at KCl [011] step edge are about 0.6 eV smaller than those on the stepped surface of NaCl (see Figure 7). We see that the band gap is determined by both the intrinsic HOMO−LUMO gap of the molecule and the relative alignment of the resonance orbital with respect to the step-edge valence states. Specifically, thanks to the relatively small HOMO−LUMO gap of the SA molecule among the presented hydroxybenzoic acids, an effective band gap of 0.90 eV has been achieved. Although the precise values of the band gaps calculated with the PW1PW hybrid functional still contain some uncertainty, the order of the predicted gap widths and the general trend presented in this study are still expected to be valid.

With the aid of Figure 7, we can now tentatively explain the contact charging effect between different alkali chlorides in terms of the reduced band gap, which serves as an essential ingredient for efficient electron excitation from the 3p states of the step edge Cl atoms to the LUMO of the adsorbate. Because the BA and *p*-SA systems show larger band gaps than the SA-adsorbate system, mobile electrons are remarkably suppressed for these two systems, because thermal excitation decays exponentially with the increasing gap width. This is exactly what has been found technologically: although mixing SA can successfully separate the NaCl and KCl, the use of BA and *p*-SA however fails.

Conclusions

In an attempt to simulate the adsorption of small organic molecules on insulating surfaces and to demonstrate the consequences on binding and electronic properties, we performed DFT calculations for the adsorption of various hydroxybenzoic acids both on perfect KCl and NaCl surfaces as well as on polar defects. As a model system for the latter, we chose pairs of polar steps.

The vdW dispersion force considerably stabilizes the binding between the molecule and the surface of wide band gap insulators. The adsorption configuration, however, is mostly determined by the local chemical and electrostatic interactions. This has also been manifested by a recent study of organic molecule adsorption on KBr(001) surfaces.[42] In the present work, we have found that the vdW interaction accounts for about half of the total adsorption energy for the adsorption on flat (100) surface. Even at the investigated polar steps, these statements remain valid. The vdW part in the molecule−surface interaction is equally given by the PBE-D method and vdW-DF, affirming the validity of both methods in the description of the long-range dispersion for the systems studied in this work.

Although the adsorption of the hydroxybenzoic acids on the KCl and NaCl surfaces are similar from the energetic point of view, the influence of surface bonding results in clear differences of alignment of the electronic levels because of varying resonances between valence bands and molecular orbitals. Contrary to the adsorbate system on NaCl surface, where the

HOMO-2 of the molecule is in resonance with the surface valence band, the resonance state from the HOMO-1 is predominant when the molecules are adsorbed on KCl surface. These resonance effects also exist for the edge states of the polar steps and are most pronounced if the molecules are adsorbed at the edge exposing the cations. This results in a strong shift of both occupied and unoccupied molecular orbitals for the molecules adsorbed there and in a remarkably reduced effective band gap of only 0.9 eV for the SA-KCl [011] stepped surface system. Thus, the importance of polar defects is demonstrated; it has a significant influence on the electronic structure and on chemical reactivity, whereas nonpolar defects have a much smaller effect.[7]

Acknowledgment. Financial support from K+S AG is greatly appreciated. We also acknowledge support by the Höchstleistungsrechenzentrum Nord (HLRN). Part of the calculation was performed on the supercomputing systems at HLRN-II.

References and Notes

(1) Burroughes, J. H.; Bradley, D. D. C.; Brown, A. R.; Marks, R. N.; Mackay, K.; Friend, R. H.; Burns, P. L.; Holmes, A. B. *Nature* **1990**, *347*, 539–541.

(2) Bloor, D. *Nature* **1992**, *356*, 19–20.

(3) Crone, B.; Dodabalapur, A.; Lin, Y. Y.; Filas, R. W.; Bao, Z.; LaDuca, A.; Sarpeshkar, R.; Katz, H. E.; Li, W. *Nature* **2000**, *403*, 521–523.

(4) Dimitrakopoulos, C. D.; Malenfant, P. R. L. *Adv. Mater.* **2002**, *14*, 99.

(5) Malaske, U.; Tegenkamp, C.; Henzler, M.; Pfnür, H. *Surf. Sci.* **1998**, *408*, 237–251.

(6) Tegenkamp, C.; Pfnür, H. *Phys. Chem. Chem. Phys.* **2002**, *4*, 2653–2659.

(7) Chen, W.; Tegenkamp, C.; Pfnür, H.; Bredow, T. *Phys. Rev. B* **2009**, *79*, 235419.

(8) Stahl, I.; Kleine-Kleffmann, U. *Kunststoffberater* **1994**, *6*, 28.

(9) Pfnür, H.; Tegenkamp, C.; Maslyuk, V.; Bredow, T. *Surf. Sci.* **2005**, *600*, 1664–1669.

(10) Langreth, D. C.; et al. *J. Phys.: Condens. Matter* **2009**, *21*, 08420315pp).

(11) Chen, W.; Tegenkamp, C.; Pfnür, H.; Bredow, T. *Phys. Chem. Chem. Phys.* **2009**.

(12) Bredow, T.; Gerson, A. R. *Phys. Rev. B* **2000**, *61*, 5194–5201.

(13) Dovesi, R.; Saunders, V.; Roetti, C.; Orlando, R.; Zicovich-Wilson, C. M.; Pascale, F.; Civalleri, B.; Doll, K.; Harrison, N.; Bush, I.; D'Arco, P.; Llunell, M. *crystal06*; University of Torino: Torino, 2006.

(14) Prencipe, M.; Zupan, A.; Dovesi, R.; Apra, E.; Saunders, V. R. *Phys. Rev. B* **1995**, *51*, 3391–3396.

(15) Grimme, S. *J. Comput. Chem.* **2006**, *27*, 1787–1799.

(16) Kresse, G.; Hafner, J. *Phys. Rev. B* **1994**, *49*, 14251–14269.

(17) Kresse, G.; Furthmüller, J. *Phys. Rev. B* **1996**, *54*, 11169–11186.

(18) Reckien, W.; Kirchner, B.; Janetzko, F.; Bredow, T. *J. Phys. Chem. C* **2009**, *113*, 10541–10547.

(19) Perdew, J. P.; Burke, K.; Ernzerhof, M. *Phys. Rev. Lett.* **1996**, *77*, 3865–3868.

(20) Perdew, J. P.; Ernzerhof, M.; Zupan, A.; Burke, K. *J. Chem. Phys.* **1998**, *108*, 1522–1531.

(21) Blöchl, P. E. *Phys. Rev. B* **1994**, *50*, 17953–17979.

(22) Kresse, G.; Joubert, D. *Phys. Rev. B* **1999**, *59*, 1758–1775.

(23) Dion, M.; Rydberg, H.; Schröder, E.; Langreth, D. C.; Lundqvist, B. I. *Phys. Rev. Lett.* **2004**, *92*, 246401.

(24) Román-Pérez, G.; Soler, J. M. *Phys. Rev. Lett.* **2009**, *103*, 096102.

(25) Mortensen, J. J.; Hansen, L. B.; Jacobsen, K. W. *Phys. Rev. B* **2005**, *71*, 035109.

(26) *Crystal Structures*, 2nd ed.; Wyckoff, W. G., Ed.; Wiley: New York, 1968; Vol. 1.

(27) Huggett, G. R.; Teegarden, K. *Phys. Rev.* **1966**, *141*, 797–802.

(28) Csonka, G. I.; Perdew, J. P.; Ruzsinszky, A.; Philipsen, P. H. T.; Lebègue, S.; Paier, J.; Vydrov, O. A.; Ángyán, J. G. *Phys. Rev. B* **2009**, *79*, 155107.

(29) Westwood, A. R. C.; Hitch, T. T. *J. Appl. Phys.* **1963**, *34*, 3085–3089.

(30) Tasker, P. W. *Phil. Mag. A* **1979**, *39*, 119–136.

(31) Hammer, B.; Hansen, L. B.; Nørskov, J. K. *Phys. Rev. B* **1999**, *59*, 7413–7421.

(32) Mattsson, A. E.; Armiento, R.; Schultz, P. A.; Mattsson, T. R. *Phys. Rev. B* **2006**, *73*, 195123.

(33) Johnston, K.; Kleis, J.; Lundqvist, B. I.; Nieminen, R. M. *Phys. Rev. B* **2008**, *77*, 121404.

(34) Anderson, P. W. *Phys. Rev.* **1961**, *124*, 41–53.

(35) Newns, D. M. *Phys. Rev.* **1969**, *178*, 1123–1135.

(36) Gadzuk, J. *Surf. Sci.* **1974**, *43*, 44–60.

(37) Gulans, A.; Puska, M. J.; Nieminen, R. M. *Phys. Rev. B* **2009**, *79*, 201105.

(38) Pojani, A.; Finocchi, F.; Goniakowski, J.; Noguera, C. *Surf. Sci.* **1997**, *387*, 354.

(39) Noguera, C. *J. Phys.: Condens. Matter* **2000**, *12*, R367.

(40) Geneste, G.; Morillo, J.; Finocchi, F.; Hayoun, M. *Surf. Sci.* **2007**, *601*, 5616.

(41) Goniakowski, J.; Finocchi, F.; Noguera, C. *Rep. Prog. Phys.* **2008**, *71*, 016501.

(42) Pakarinen, O. H.; Mativetsky, J. M.; Gulans, A.; Puska, M. J.; Foster, A. S.; Grutter, P. *Phys. Rev. B* **2009**, *80*, 085401.

JP909308K